Magnetization curves of an Fe/Gd multilayer film calculated from Gd magnetization depth profiles determined by resonant x-ray magnetic scattering

2002 J. Phys.: Condens. Matter 14 5289

(http://iopscience.iop.org/0953-8984/14/21/304)

INSTITUTE OF PHYSICS PUBLISHING JOURNAL OF PHYSICS: CONDENSED MATTER

J. Phys.: Condens. Matter **14** (2002) 5289–5301 PII: S0953-8984(02)30261-3

Magnetization curves of an Fe/Gd multilayer film calculated from Gd magnetization depth profiles determined by resonant x-ray magnetic scattering

N Hosoito[1,4], **H Hashizume**[2] **and N Ishimatsu**[3]

[1] Institute for Chemical Research, Kyoto University, Uji, Kyoto-fu 611-0011, Japan
[2] Research and Education Centre for Materials Science, Nara Institute of Science and Technology, Ikoma 630-0101, Japan
[3] Kansai Laboratory, Japan Atomic Energy Research Institute, Mikazuki, Hyogo 679-5148, Japan

E-mail: hosoito@scl.kyoto-u.ac.jp

Received 17 October 2001
Published 16 May 2002
Online at stacks.iop.org/JPhysCM/14/5289

Abstract

Magnetization-versus-applied-field curves $M(H)$ are calculated for an $[Fe(3.48\ nm)/Gd(5.43\ nm)]_{15}$ multilayer film using the Gd magnetization depth profiles derived from the resonant x-ray magnetic scattering data collected with an applied field of 2.4 kOe. Stable magnetic structures for other field strengths are calculated by minimizing the sum of the Fe–Fe, Gd–Gd and Gd–Fe exchange energies and the Zeeman energy in a temperature range of 140–240 K. The calculated curves fit very well the slowly rising $M(H)$ curves observed at temperatures between 140 and 200 K, where the Gd layers are ferromagnetic, over a wide field range up to 50 kOe on adjusting a molecular-field constant for the Fe–Gd interfaces, the only one free parameter used. The concave magnetization depth profiles in the Gd layers are essential to reproduce the observed $M(H)$ curves. The discrepancies between the observed and calculated curves in low-field regions represent the limitation of the single-magnetic-domain model used in the calculation.

1. Introduction

The magnetic structure of Fe/Gd multilayers is the so-called aligned state or the twisted state, depending on the strength of the in-plane applied field H and temperature T. In the aligned state, the magnetic moments of the Fe and Gd layers line up with the applied field, while they are canted from the field direction in the twisted state. This was first shown by theoretical investigations, which enabled H–T phase diagrams to be calculated [1–3]. Experimental confirmations followed that used magnetization [4, 5] and magnetoresistance

[4] Author to whom any correspondence should be addressed.

measurements [4,6], Mössbauer spectroscopy [7], neutron diffraction [8,9] and x-ray magnetic circular dichroism (XMCD) [10–12]. The intriguing temperature and field behaviours of the magnetic structure of Fe/Gd multilayers originate in the significantly different temperature dependence of the Fe and Gd moments and are determined by a balance of the Zeeman energy and the exchange energy.

In a previous paper [13], we used the resonant x-ray magnetic scattering (RXMS) technique at a synchrotron source to determine the magnetic structures of an Fe/Gd multilayer in the Fe-aligned state and the twisted state. The advantages of the RXMS over other techniques reside in its element specificity and high momentum and real-space resolutions. By measuring the specular reflectivity with x-rays of energies tuned close to the absorption edges of Fe and Gd, we separately explored the magnetization depth profiles of the Fe and Gd layers to subnanometre resolutions. The RXMS technique thus possesses the element specificity of the XMCD technique and the spatial resolution of the neutron diffraction technique. We successfully isolated the magnetic charge interference scattering from the dominant charge (Thomson) scattering using the helicity flip technique with circularly polarized probing x-rays. The difference reflectivity profiles measured with x-rays of + and − helicities were fitted using the extended Parratt recursion formula to map the distributions of size and canting angle of local Gd magnetizations across the 5.4 nm thick Gd layer at $H = 2.4$ kOe, $T = 140$–300 K. To the best of our knowledge, this is the first high-resolution experimental determination of the Gd magnetic structures.

In the present paper, we calculate magnetization-versus-applied-field curves $M(H)$ from the depth profiles of Gd magnetizations given in [13] and compare the results with the observed $M(H)$. If consistent fits are accomplished at various temperatures, the magnetization depth profiles determined by the RXMS technique will acquire support and the technique will be placed on a firm basis. Since the Gd magnetizations were given in relative units, we shall first scale them into absolute units such as emu cm^{-3} or Bohr magnetons (μ_B) per atom, in section 3.1. This will be followed by a description of the method that we used to calculate $M(H)$ curves in section 3.2. The results are compared with the measured curves in section 3.3 and a discussion will appear in section 4. We start with the sample preparation in section 2.

2. Sample preparation and chemical structure

The sample preparation and evaluation are described in [13]. We give a brief summary here. Fe/Gd multilayer films were grown in an ultrahigh-vacuum deposition chamber (3×10^{-7} Pa) equipped with electron-gun evaporators and a quartz thickness monitor. The evaporation sources are iron and gadolinium metal ingots, which were deposited at rates of 1.2–1.8 nm min^{-1} on a Si(111) substrate at room temperature. A series of multilayers with slightly different Fe and Gd layer thicknesses were grown to allow us to work out combinations suited to x-ray scattering experiments. After trial runs, we selected a stacking structure of Si substrate/[Gd(5.2 nm)/Fe(3.5 nm)]$_{15}$/Si(3.5 nm). The capping Si layer is present to prevent oxidation. Figure 1 shows a charge x-ray specular reflectivity profile recorded at a Cu Kα source. Sharp superlattice Bragg peaks are observed up to the fourth order ($q_z = 2.82$ nm^{-1}), demonstrating a high multilayer order in the sample. We point out that the number of observable Bragg peaks is important, since it determines the depth resolution achievable in the magnetic structure analysis. The charge reflectivity profile in figure 1 was fitted under the assumption of chemically sharp (no interdiffusion), topographically wavy interfaces. A least-squares fit simultaneously determined $t_{\mathrm{Fe}} = 3.48 \pm 0.11$ nm and $\rho^*_{\mathrm{Fe}} = 0.88 \pm 0.05$ for the thickness and density of the Fe layers, respectively, $t_{\mathrm{Gd}} = 5.43 \pm 0.11$ nm and $\rho^*_{\mathrm{Gd}} = 0.97 \pm 0.06$ for those of the Gd layers, respectively, and $\sigma_{\mathrm{Fe-Gd}} = 0.81 \pm 0.06$ nm for the root mean square roughness

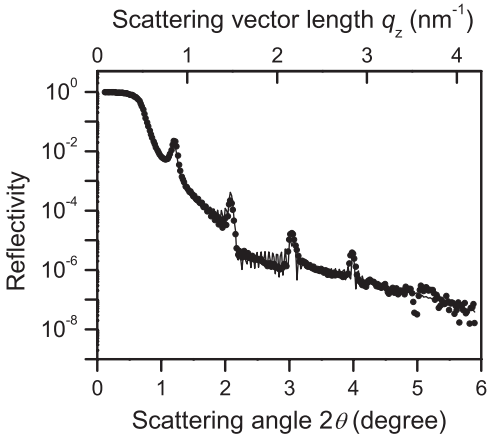

Figure 1. The charge specular reflectivity profile for the [Fe(3.58 nm)/Gd(5.43 nm)]$_{15}$ multilayer sample observed with Cu Kα x-rays. The solid curve shows a fit.

of the Fe–Gd interfaces. The densities are relative to those for bulk bcc Fe and hcp Gd. These values, used in the analysis of the RXMS data [13], will be employed in the calculation of magnetization curves in this paper. The high-angle x-ray diffraction pattern indicated a clear hcp Gd(0002) peak and a trace of bcc Fe(110) peak. We measured magnetization-versus-applied-field curves $M(H)$ using an Fe/Gd multilayer grown on a 12.5 μm thick Kapton film in the same deposition run as the x-ray sample. The $M(H)$ curves were recorded at $T = 5$–300 K using a SQUID magnetometer (Quantum Design MPMS 5). Raw magnetization data are sensitive to trace magnetic impurities in a substrate material, especially at low temperatures. The SQUID signal of a Kapton substrate is smaller than that of a Si substrate. This explains why we used the Fe/Gd sample grown on a Kapton film in magnetization measurements, in place of the one grown on the Si substrate. The two samples have similar magnetic properties, as discussed in [13].

3. Calculation of magnetization curves

3.1. Gd magnetization depth profile

In the previous paper [13], we determined $S_p^{\parallel}$ and $S_p^{\perp}$, Gd magnetizations of sublayer p ($p =$ 1–20) parallel and perpendicular to the applied-field direction, for a [Fe(3.5 nm)/Gd(5.4 nm)]$_{15}$ multilayer film placed in a magnetic field of 2.4 kOe. The RXMS technique gave $S_p^{\parallel}$ and $S_p^{\perp}$ at various temperatures on a common scale but hardly allowed their sizes to be evaluated on an absolute scale. We calculated the mean parallel magnetizations $\langle S_p^{\parallel} \rangle$ of the Gd layer in the Fe-aligned state and compared them with the Gd magnetizations estimated from the total magnetizations measured with a SQUID magnetometer. This yielded the relationship $M_{\mathrm{Gd}} = 559.4\langle S_p^{\parallel} \rangle$ (emu cm^{-3}), where M_{Gd} is the Gd magnetization per unit volume of the Gd layer [13].

Even though $M_{\mathrm{Gd}} = 559.4\langle S_p^{\parallel} \rangle$ was derived using $S_p^{\parallel}$ for the Fe-aligned state, this is a universal scaling law applicable to $S_p^{\parallel}$ and $S_p^{\perp}$ for the aligned and twisted states for all temperatures. In this paper, we use this law to estimate the sizes of depth-dependent Gd magnetization vectors μ_p^{Gd} for the twisted state, as well as for the Fe-aligned state. Synthesizing $S_p^{\parallel}$ and $S_p^{\perp}$ shown in figure 8 of [13], we obtain $\mu_p^{\mathrm{Gd}} = 7.55 \times \frac{559.4}{2056}\sqrt{(S_p^{\parallel})^2 + (S_p^{\perp})^2}$ for the

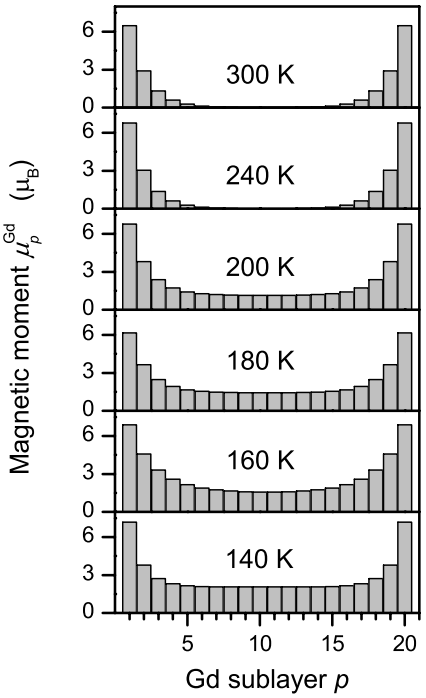

Figure 2. The depth profile of the magnitude of the Gd magnetization vector $\boldsymbol{\mu}_p^{\mathrm{Gd}}$ synthesized from observed $\langle S_p^{\parallel}\rangle$ and $\langle S_p^{\perp}\rangle$ and placed on the absolute scale by combining the macroscopic magnetization data.

magnitudes of local Gd magnetization vectors in units of the Bohr magneton (μ_B), where 2056 is the saturation magnetization of the Gd layer in emu cm^{-3} corrected for its density (corresponding to 7.55 μ_B per atom). The results are plotted in figure 2 for six temperatures. The profiles obtained are concave at all temperatures: large magnetizations are located at the Fe interfaces ($p = 1$ and 20) and the core of the Gd layer ($p \approx 10$) has vanishing or small magnetizations. The interface magnetizations are virtually temperature independent in the range 6.2–7.2 μ_B, which compares well with 7.55 μ_B, the full atomic moment of Gd. Clearly, the large interface magnetizations are induced by the molecular field from the adjacent Fe moments. In contrast, the magnetizations in the core of the Gd layer, $\mu_{\mathrm{core}}^{\mathrm{Gd}}$, show a linear temperature dependence $\mu_{\mathrm{core}}^{\mathrm{Gd}} \propto (1 - T/T_C)$ with $T_C = 214$ K, indicating that the core magnetizations are spontaneous, not induced by the Fe molecular field. The linear temperature dependence of $\mu_{\mathrm{core}}^{\mathrm{Gd}}$ shows that even for the core sublayer ($p = 10$), a standard molecular-field theory does not describe the temperature dependence of the Gd magnetization. We pointed out in [13] that the thin Gd layer has a Curie temperature much lower than bulk Gd ($T_C = 272$ K).

3.2. Calculation of M(H) curves

On the basis of the molecular-field theory, Camley and co-workers [1–3] developed a formalism minimizing the free energy, which is straightforward and valid at finite temperatures. It includes, however, cumbersome calculations of self-consistent spin vector configurations and the partition function Z at finite temperatures. We will adopt here a simpler formalism developed by Motokawa and Dohnomae [14, 15] that minimizes energy instead of free energy.

Motokawa and Dohnomae considered the exchange energy and the Zeeman energy, but neglected the entropy S in the free energy $F = E - TS$. Furthermore, their formalism assumes fixed magnitudes of magnetic moments, resulting in only the orientations being variable parameters. Results obtained by Motokawa and Dohnomae's approach are therefore accurate only at $T = 0$ K. Nevertheless, this approach has been proven to reproduce many features observed in Fe/Gd multilayers at low and moderate temperatures. We modify Motokawa and Dohnomae's formula by explicitly considering the number of nearest-neighbour atoms in the expression for the exchange energy [4]. Our calculation starts with the following formula:

$$E = -\frac{1}{2}\sum_i \frac{1}{z_i}(n_{i-1,i}A_{i-1,i}\boldsymbol{M}_{i-1} + n_{i,i}A_{i,i}\boldsymbol{M}_i + n_{i+1,i}A_{i+1,i}\boldsymbol{M}_{i+1}) \cdot \boldsymbol{M}_i a_i \Big/ \sum_i a_i - \sum_i \boldsymbol{M}_i \cdot \boldsymbol{H}_{\text{ext}} a_i \Big/ \sum_i a_i. \quad (1)$$

Magnetic energy E per unit volume is given by the sum of the exchange energy (the first term) and the Zeeman energy (the second term). $\boldsymbol{M}_i$ is the magnetization (emu cm^{-3}) of atom plane i. $n_{j,i}$ is the number of atoms in plane j in the nearest-neighbour positions for an atom in plane i, where $j = i-1$, i or $i+1$. $z_i = n_{i-1,i} + n_{i,i} + n_{i+1,i}$ is the total nearest-neighbour atom number for an atom in plane i. The symbol A stands for the molecular-field constant. $A_{j,i}\boldsymbol{M}_j$ is the molecular field (in Oe) acting on $\boldsymbol{M}_i$ from $\boldsymbol{M}_j$. a_i is the spacing of atom plane i. $\boldsymbol{H}_{\text{ext}}$ is an external field applied in the film plane. The summation in formula (1) runs over all atom planes in one Fe/Gd bilayer. That is, we assume that the fifteen Fe/Gd bilayers in our $[\text{Fe/Gd}]_{15}$ multilayer have the same magnetic structure. Magnetization $\boldsymbol{M}_i$ is expressed in terms of magnitude M_i and angle θ_i measured from the applied-field direction, i.e. $\boldsymbol{M}_i = (M_i, \theta_i)$. When the M_i are replaced by the known magnetizations, magnetic energy E becomes a function of a set of angles θ_i. A stable magnetic structure may be found by setting $\partial E/\partial\theta_i = 0$ for all i. This leads to the following recursion formula:

$$\frac{1}{2}\left(\frac{n_{i+1,i}a_i}{z_i} + \frac{n_{i,i+1}a_{i+1}}{z_{i+1}}\right)A_{i,i+1}M_iM_{i+1}\sin(\theta_{i+1} - \theta_i) = \frac{1}{2}\left(\frac{n_{i,i-1}a_{i-1}}{z_{i-1}} + \frac{n_{i-1,i}a_i}{z_i}\right)A_{i-1,i}M_{i-1}M_i\sin(\theta_i - \theta_{i-1}) + M_iH_{\text{ext}}a_i\sin\theta_i. \quad (2)$$

Equation (2) indicates that when two angles θ_{i-1} and θ_i are given, θ_{i+1} is calculated. Namely, two initial angles determine all other angles. Following Motokawa and Dohnomae [14, 15], we take for the initial angles the angle of an interface Fe magnetization, $\theta_{\text{int}}^{\text{Fe}}$, and that of an interface Gd magnetization, $\theta_{\text{int}}^{\text{Gd}}$. We assume symmetric distributions of θ_i^{Fe} and θ_i^{Gd} in each layer. Magnetization curves can be calculated in the following way. We arbitrarily choose initial angles $\theta_{\text{int}}^{\text{Fe}}$ and $\theta_{\text{int}}^{\text{Gd}}$ and calculate all angles θ_i using equation (2). The magnetic energy $E(\theta_{\text{int}}^{\text{Fe}}, \theta_{\text{int}}^{\text{Gd}})$ is then evaluated from formula (1). The angles $\theta_{\text{int}}^{\text{Fe}}$ and $\theta_{\text{int}}^{\text{Gd}}$ are slightly varied, $\theta_{\text{int}}^{\text{Fe}} \rightarrow \theta_{\text{int}}^{\text{Fe}} + \Delta\theta_{\text{int}}^{\text{Fe}}$ and $\theta_{\text{int}}^{\text{Gd}} \rightarrow \theta_{\text{int}}^{\text{Gd}} + \Delta\theta_{\text{int}}^{\text{Gd}}$, new θ_i are calculated and the energy $E(\theta_{\text{int}}^{\text{Fe}} + \Delta\theta_{\text{int}}^{\text{Fe}}, \theta_{\text{int}}^{\text{Gd}} + \theta_{\text{Int}}^{\text{Gd}})$ is evaluated. If $E(\theta_{\text{int}}^{\text{Fe}} + \Delta\theta_{\text{int}}^{\text{Fe}}, \theta_{\text{int}}^{\text{Gd}} + \Delta\theta_{\text{int}}^{\text{Gd}}) < E(\theta_{\text{int}}^{\text{Fe}}, \theta_{\text{int}}^{\text{Gd}})$, the angles $\theta_{\text{int}}^{\text{Fe}} + \Delta\theta_{\text{int}}^{\text{Fe}}$ and $\theta_{\text{int}}^{\text{Gd}} + \Delta\theta_{\text{int}}^{\text{Gd}}$ are accepted as new initial angles. We repeat this procedure until a minimal $E(\theta_{\text{int}}^{\text{Fe}}, \theta_{\text{int}}^{\text{Gd}})$ is obtained. Once the most stable magnetic structure is acquired for a given applied-field strength H_{ext}, the magnetization along the field direction is evaluated according to

$$M(H_{\text{ext}}) = \sum_i M_i a_i \cos\theta_i \Big/ \sum_i a_i. \quad (3)$$

Repeating this procedure for various applied-field values produces a magnetization curve $M(H_{\text{ext}})$ for the set of M_i employed.

Table 1. Parameter values used in the calculation.

	A	z	$n_{i\pm1,i}$	$n_{i,i}$	a (nm)
Fe	7168	8	2	4	0.203
Gd	666	12	3	6	0.289

The x-ray diffraction pattern indicates a bcc (110) stacking for the Fe layer and a hcp (0001) stacking for the Gd layer. It is a good approximation to assume a uniformly magnetized Fe layer. All of the M_i in the Fe layer are then fixed at 1531 emu cm^{-3} (corresponding to 2.22 μ_B per atom), which includes $\rho^*_{\mathrm{Fe}} = 0.88$, for all temperatures and applied-field strengths H_{ext}. For the Gd magnetization, we use the depth profiles given in figure 2 for all H_{ext}, sampled at the interplanar spacing of Gd(0001)[5], $a_i = 0.289$ nm. All M_i are now to hand, which allows us to calculate $M(H_{\mathrm{ext}})$ for each temperature of figure 2. Table 1 lists the parameter values we used. The molecular-field constants $A_{\mathrm{Fe,Fe}}$ and $A_{\mathrm{Gd,Gd}}$ were estimated from $A = 3k_BT_C/Ng^2S(S+1)\mu_B^2$, where k_B is the Boltzmann constant and T_C the Curie temperature. We used the bulk Curie temperatures for T_C (1043 K for Fe and 292 K for Gd) and took into account the deviations of atom number density N in the multilayer from the bulk values. The g-factor is 2 and the spin S was taken to be $gS = 2.22$ for Fe and 7.55 for Gd. The molecular-field constant at the Fe–Gd interface, $A_{\mathrm{Fe,Gd}}$, is a free variable parameter in the data fitting.

3.3. Comparison with experimental M(H)

Figure 3 compares the calculated $M(H)$ curves with the observed magnetizations for $T =$ 180 K. The solid and dotted curves show the $M(H)$ calculated using $A_{\mathrm{Fe,Gd}} = -1000$, -800, -700, -600 and -400. The negative $A_{\mathrm{Fe,Gd}}$-values indicate the antiferromagnetic interaction between Fe and Gd. The $M(H)$ curve for $A_{\mathrm{Fe,Gd}} = -700$ fits very well the observed magnetizations over a wide applied-field range up to 50 kOe. The small discrepancy in the low-field region arises from the limitation of the single-magnetic-domain model. A discussion is given on this point in a later section of this paper.

The molecular-field constant at the interface, $A_{\mathrm{Fe,Gd}}$, is proportional to the exchange coupling constant for Fe and Gd. Since the exchange coupling constant does not depend on temperature, $A_{\mathrm{Fe,Gd}} = -700$ must equally well explain the magnetizations observed at temperatures other than 180 K. This is evidenced in figure 4. In fact, the calculated curves agree well with the observations for $T = 140$, 160, 180 and 200 K. In contrast, the calculated curve does not fit the data at $T = 240$ K. The failure is accounted for as follows. As indicated in section 3.1, the Curie temperature at the core of the Gd layer is 214 K, which is much lower than the bulk T_C (292 K). The core of the Gd layer is paramagnetic at 240 K, as seen from the missing spontaneous magnetization in figure 2. When the applied field becomes strong, non-negligible magnetizations are induced in the paramagnetic Gd layer. On the other hand, our calculation assumes constant magnetizations regardless of the applied-field strength. That is, each Gd sublayer p holds a fixed magnitude of the magnetization $m_p(H) = m_p(H = 0) + \Delta m_p(H)$ with $\Delta m_p(H) = 0$. For paramagnetic Gd layers, we have $m_p(H = 0) = 0$ and non-zero field-dependent $\Delta m_p(H)$. In this situation, our calculation should fail at $T = 240$ K. Note

[5] We multiplied the depth profiles of figure 2 by factors of 1.00–1.15 to take account of the deviations of $\langle\mu_p^{\mathrm{Gd}}\rangle$ from the best-fitted straight line and the fractional atom-plane numbers given by $t_{\mathrm{Fe}}/a_{\mathrm{Fe}}$ and $t_{\mathrm{Gd}}/a_{\mathrm{Gd}}$. We assumed 17 Fe(110) planes ($\alpha_{\mathrm{Fe}} = 0.203$ nm) and 19 Gd(0001) planes ($a_{\mathrm{Gd}} = 0.289$ nm) in a unit Fe/Gd bilayer. Calculations using 20 Gd planes, in accordance with the p-number in figure 2, with $a_{\mathrm{Gd}} = 0.272$ nm, produced very similar $M(H)$ curves. We confirmed that the choice of a_i for the Gd planes does not critically affect the calculation results.

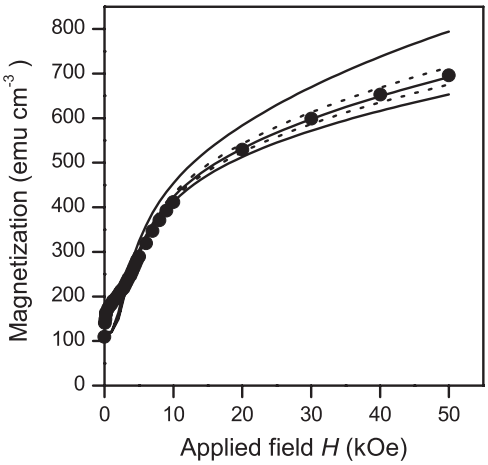

Figure 3. Observed (closed circles) and calculated (solid and dotted curves) magnetizations for the Fe/Gd multilayer at 180 K. The applied-field direction is in the film plane. The interface molecular-field constant $A_{\mathrm{Fe,Gd}}$ equals -400 (uppermost solid curve), -600, -700 (middle curve), -800 and -1000 (bottom curve). The middle solid curve fits the data best.

that the good agreement of the calculated $M(H)$ curves with the observed magnetizations is accomplished for $T = 140$–200 K with only one variable parameter, $A_{\mathrm{Fe,Gd}}$. This evidences the reliability and consistency of the magnetic structures determined by the RXMS technique. We point out that $A_{\mathrm{Fe,Gd}} = -700$, providing good fits of the observed $M(H)$ curves, is larger in absolute value than $A_{\mathrm{Gd,Gd}} = 666$ and much smaller than $A_{\mathrm{Fe,Fe}} = 7168$ given in table 1.

4. Discussion

In the calculation of the $M(H)$ curves, we made a few assumptions:

(1) all Fe sublayers have the bulk magnetic moment (2.22 μ_B) independent of temperature;
(2) at a given temperature, the magnitudes of both Fe and Gd sublayer magnetizations are constant against variable applied-field strength; and
(3) both Fe and Gd magnetizations are fixed in the film plane.

As regards assumption 1, Takanashi *et al* estimated the Fe and Gd magnetic moments at 4.2 K from the dependence on the multilayer period (λ) of the residual magnetization [4]. They assumed that the Gd moment at 4.2 K was independent of λ and attributed the λ-dependent residual magnetization to the varied Fe moment at 4.2 K. The estimated moment of their 3.7 nm thick Fe layers is about 1.5 μ_B, which is very small compared with the value that we assumed (2.22 μ_B). Our assumption is based on the ^{57}Fe Mössbauer spectrum for our multilayer in the zero field, that showed a hyperfine field of 320.8 ± 1.1 kOe at room temperature [13]. This is very close to the bulk value (330 kOe). The 3.48 nm thick Fe layers in our $[\mathrm{Fe/Gd}]_{15}$ multilayer are thus likely to have the bulk moment. Furthermore, the narrow widths of the Mössbauer peaks exclude a wide distribution of the Fe moment. Assumption 1 is thus experimentally supported.

The assumption of fixed magnetization magnitudes (assumption 2) is an acceptable one, because the molecular field acting in ferromagnets is much stronger than the applied field used in this study. For instance, in a Gd layer having a third of the saturation magnetization at 0 K, the molecular field is as high as 456 kOe ($=666 \times 2056/3$). As all Gd atoms are always

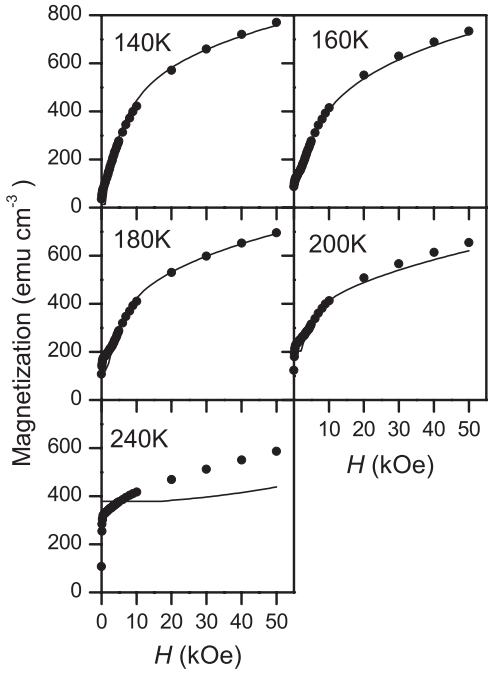

Figure 4. Observed (circle) and calculated (curve) magnetization curves for the Fe/Gd multilayer at $T = 140$, 160, 180, 200 and 240 K. The calculated curves assume $A_{\mathrm{Fe,Gd}} = -700$.

placed in such a high effective field, no practical change would take place in the size of the Gd magnetization when the external-field strength varies from 0 to 50 kOe, i.e. $\Delta m_p(H) = 0$, except at temperatures close to T_C.

It is reported that amorphous Fe–Gd alloy films show a perpendicular magnetization [16]. However, we have some experimental evidence supporting assumption 3 for our sample. First of all, the six lines in the Mössbauer spectrum observed from our $[\mathrm{Fe/Gd}]_{15}$ multilayer show the 3:4:1:1:4:3 intensity ratio. This indicates that the Fe moments are directed parallel to the film plane. For further support, we compare the magnetization curves measured with applied fields parallel and perpendicular to the film plane (figure 5). The magnetization measured with an in-plane applied field, $M(H_\parallel)$, is always larger than that measured with a perpendicular applied field, $M(H_\perp)$, for the same field strength ($H_\parallel = H_\perp$). Furthermore, we note that below 160 K, the $M(H_\parallel)$ and $M(H_\perp)$ in figure 5 are related by $M(H_\parallel) \approx M(H_\perp - 4\pi M(H_\perp))$. This indicates that the demagnetization field accounts for the difference between $M(H_\parallel)$ and $M(H_\perp)$. In other words, our Fe/Gd multilayer has no perpendicular magnetic anisotropy. We conclude that both Fe and Gd magnetizations are in the film plane at all temperatures.

It is instructive to calculate the $M(H)$ curves for a uniformly magnetized Gd layer and to compare the results with the observation. The comparison will highlight the significance of the concave-shaped magnetization depth profiles of figure 2. The solid curves in figure 6 show the $M(H)$ curves calculated for a uniform Gd magnetization of 2.89 μ_B, equivalent to the mean of the concave profile for $T = 180$ K in figure 2. The solid curves, weakly depending upon the molecular-field constant $A_{\mathrm{Fe,Gd}}$, show more rapid rises than the $M(H)$ curve for the concave magnetization, shown by a broken line ($A_{\mathrm{Fe,Gd}} = -700$). It is probably impossible to fit the observed magnetizations (closed circles) by a uniform-magnetization model as long as $A_{\mathrm{Fe,Gd}}$ is the only variable parameter.

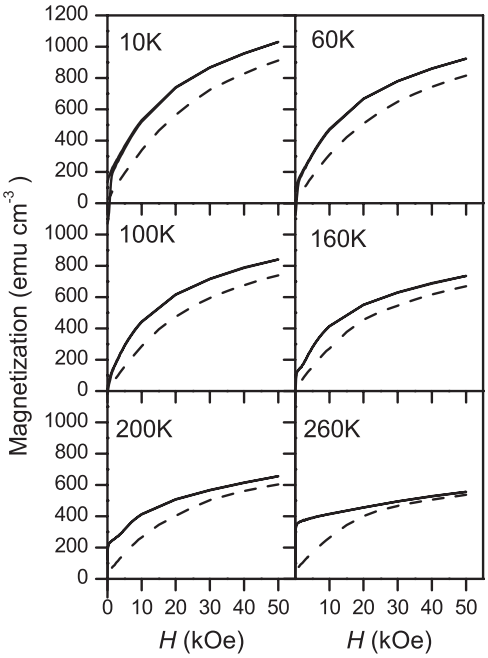

Figure 5. Comparing the magnetization curves measured with in-plane (solid curves) and perpendicular (broken curves) applied fields at various temperatures.

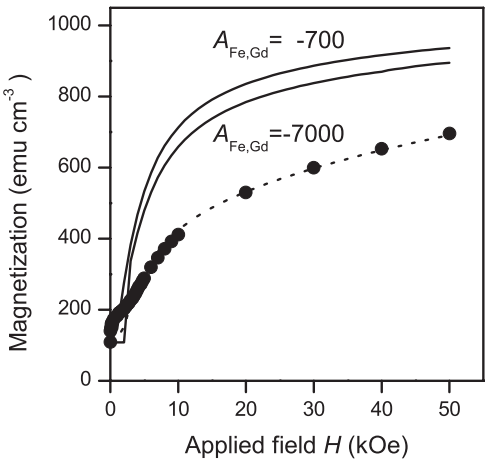

Figure 6. Comparing the magnetization curves calculated from the uniform model (solid curves) and the concave model (dotted curve) of the Gd magnetization depth profile. The dotted curve assumes $A_{\mathrm{Fe,Gd}} = -700$. Closed circles show the magnetizations observed at 180 K.

The cause of the unsuccessful fitting by the uniform-magnetization model becomes clear when we look into the rotation behaviour of local Gd moments. Figure 7 shows the magnitudes and orientations of local Fe and Gd moments calculated from the concave Gd magnetization profile for $T = 180$ K. The long Gd magnetization vectors are located close to the Fe interface, while the short vectors are in the core of the Gd layer. Figure 7(a) shows the magnetic structure

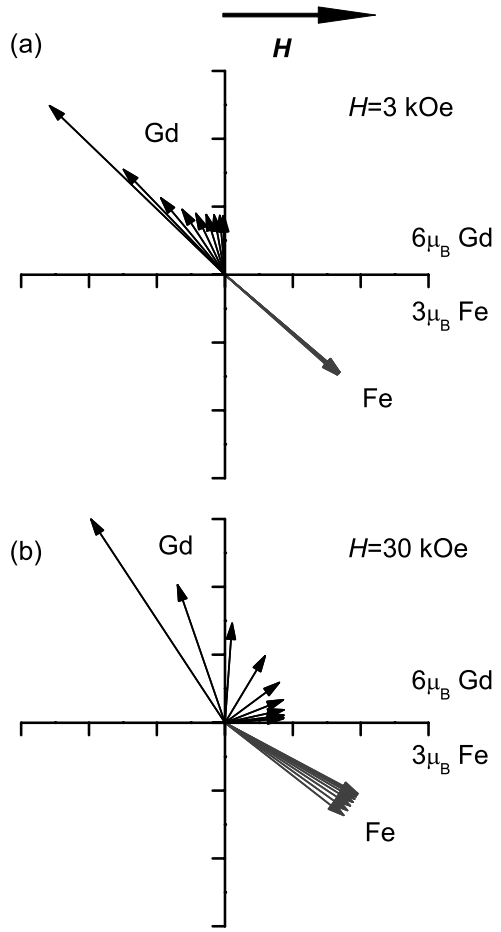

Figure 7. In-plane orientations of local Fe and Gd magnetic moments calculated for $T = 180$ K. (*a*) Applied field $H = 3$ kOe, (*b*) $H = 30$ kOe. The arrow length is proportional to the moment size. The long Gd vectors represent the Gd magnetizations at the Fe interfaces, while the short arrows represent those in the core of the Gd layer. The Fe vectors are shown on a doubled scale. The applied field H is directed from left to right.

somewhat after the Fe-aligned $\rightarrow$ twisted transition ($H = 3$ kOe), while the configuration for a higher field ($H = 30$ kOe) is shown in figure 7(*b*). The Gd vectors change their orientations remarkably as the applied field increases ($H = 3 \rightarrow 30$ kOe), except for the interface moments that are virtually pinned down by the antiferromagnetic exchange interaction with the Fe moments. The interior Gd moments, located away from the interface, are more free to rotate towards the applied-field direction to reduce the Zeeman energy. The Fe magnetization vectors do not rotate much and stay in a narrow angle range even when the external field is increased up to 30 kOe. This is because of the large $A_{\mathrm{Fe,Fe}}$ constant (see table 1). A small angle made by the adjacent Fe moments suffices to produce a large increase in the Fe–Fe exchange energy. These observations indicate that the increase of observed magnetization M with increased external field H is almost entirely accounted for by the rotating Gd moments. Note that the interface Gd magnetizations have negative components along the field direction, whereas those in deep sublayers make positive contributions to M as H increases at 180 K. If we replace the concave magnetization depth profile with a uniform one of equal mean strength, the interface

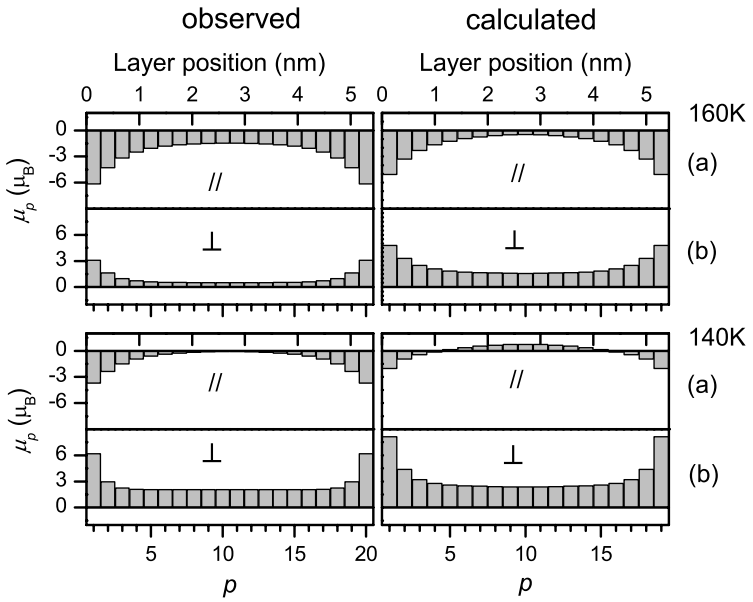

Figure 8. Gd magnetization depth profiles derived from the x-ray scattering data (left panels) and the energy calculation (right panels). (*a*) Parallel component, (*b*) perpendicular component. Top panels for $T = 160$ K and bottom panels for $T = 140$ K.

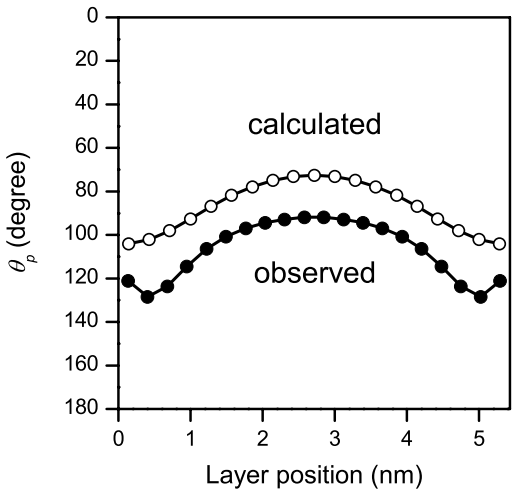

Figure 9. Observed and calculated angles θ_p between the Gd sublayer moment and the applied-field direction at $T = 140$ K.

Gd vectors become smaller in length and the interior Gd vectors become larger. This leads to a more rapidly rising $M(H)$ curve for an Fe/Gd multilayer with a uniformly magnetized Gd layer.

The Gd magnetizations of interior sublayers are not significantly affected by the Fe–Gd exchange interaction at the interface. This explains the weak $A_{\mathrm{Fe,Gd}}$-dependence of the $M(H)$ curves calculated for the uniform-magnetization model (see figure 6), in which a larger fraction

of the total magnetization is located away from the interface than in the concave magnetization model. The argument up to this point indicates that the concave magnetization depth profile in the Gd layer is crucial for reproducing the slowly rising $M(H)$ curves. We stress that a standard molecular-field theory does not allow the concave magnetization depth profile to be calculated, or its temperature dependence. This suggests that the $M(H)$ and $M(T)$ curves cannot be reproduced unless the Gd magnetization depth profiles are known to be concave. Indeed, the authors of [4] failed to reproduce the $M(T)$ curves, although their $M(H)$ curves are reasonably well fitted at 4.2 K.

It is worthwhile to calculate the parallel and perpendicular components of the Gd magnetization, $\mu_p^{\parallel}$ and $\mu_p^{\perp}$, from μ_p^{Gd} of figure 2 using the θ_p giving the best-fit $M(H)$ curves, and to compare the results with those of figure 8 in [13]. Figure 8 of this paper does this at $T = 160$ and 140 K. The calculated profiles are similar to the observed ones, with the distinctive decay rates of the parallel and perpendicular magnetizations nicely reproduced. The calculated profiles are slightly shifted upwards, however. That is, the calculated magnetizations make larger angles to the reversed applied-field direction than the RXMS results. This is clearly seen in figure 9 that shows the plots of θ_p, the angle formed by the magnetic moment of sublayer p to the field direction, for $T = 140$ K. The disagreement regarding the θ_p-angles arises from the deviation of the calculated critical field H^* for the aligned $\rightarrow$ twisted transition from the one (H_{inf}) estimated from the inflection point in the observed $M(H)$ curves. H^*-fields are commonly smaller than H_{inf}-fields by about 1 kOe at all temperatures. Hence, if magnetization profiles are compared at the same field strength near H_{inf}, the calculated magnetizations rotate from the reversed applied-field direction by greater angles: the Fe/Gd multilayer is already in a twisted state. The deviation of H^* from H_{inf} may originate from the oversimplified model of the Gd magnetic structure. The observed $M(H)$ curves show $\mathrm{d}M/\mathrm{d}H > 0$ below H_{inf}, while $\mathrm{d}M/\mathrm{d}H = 0$ in the model calculation. The fact that $\mathrm{d}M/\mathrm{d}H > 0$ indicates that in the multilayer, there are Fe and Gd magnetizations non-collinear to the applied field even in the aligned state. In order to properly calculate the magnetic structure of the Fe/Gd multilayer for low applied fields, we have to consider magnetic domain structures. The analysis of the RXMS data described in [13] and our fitting of the magnetization curves were carried out using a single-domain model. We stress that the single-domain model is a good approximation for medium- and high-field regions because the volume of energetically unfavourable domains becomes smaller with increasing applied field. Considering the relative importance of multidomain structures at low field strengths, we regard the observed and calculated magnetization profiles in figure 8 as being in reasonable agreement.

In summary, it is rather surprising that the simple formulae (1) and (2) combined with the experimentally determined Gd magnetization depth profiles fit the magnetization curves $M(H)$ so well over the wide applied-field range. The less successful fits in the low-field region represent the limitation of the single-magnetic-domain model. The reasonable agreement of the calculated $M(H)$ curves with the observed ones is strong support for the concave magnetization depth profiles in the Gd layer obtained from the RXMS measurements.

Acknowledgments

This work was supported by Grant-in Aids, Ministry of Education, Science and Culture, No 13650721 and No 13640361, and by the Japan–Korea Cooperative Science Programme organized by JSPS and KOSEF. NH and HH appreciate the support given to them by the Collaborative Research Project of the Materials and Structure Laboratory, Tokyo Institute of Technology.

References

[1] Camley R E and Tilley D R 1988 *Phys. Rev.* B **37** 3413
[2] Camley R E 1989 *Phys. Rev.* B **39** 12 316
[3] LePage J G and Camley R E 1990 *Phys. Rev. Lett.* **65** 1152
[4] Takanashi K, Kamiguchi Y, Fujimori H and Motokawa M 1992 *J. Phys. Soc. Japan* **61** 3721
[5] Cherifi K, Dufour C, Marchal G, Mangin Ph and Hubsch J 1992 *J. Magn. Magn. Mater.* **104–7** 1833
[6] Vaezzadeh M, George B and Marchal G 1994 *Phys. Rev.* B **50** 6113
[7] Sajieddine M, Bauer Ph, Cherifi K, Dufour C, Marchal G and Camley R E 1994 *Phys. Rev.* B **49** 8815
[8] Dufour C, Cherifi K, Marchal G, Mangin Ph and Hennion M 1993 *Phys. Rev.* B **47** 14 572
[9] Hahn W, Loewenhaupt M, Huang Y Y, Felcher G P and Parkin S S P 1995 *Phys. Rev.* B **52** 16 041
[10] Itoh F, Nakamura M, Sakurai H, Kiriake H, Nawate M, Honda S and Kawata H 1993 *Japan. J. Appl. Phys. Suppl.* 2 **32** 326
[11] Itoh F, Nakamura M and Sakurai H 1993 *J. Magn. Magn. Mater.* **126** 361
[12] Koizumi A, Takagaki M, Suzuki M, Kawamura K and Sakai N 2000 *Phys. Rev.* B **61** R14 909
[13] Ishimatsu N, Hashizume H, Hamada S, Hosoito N, Nelson C S, Venkataraman C T, Srajer G and Lang J C 1999 *Phys. Rev.* B **60** 9596
[14] Motokawa M 1990 *Prog. Theor. Phys. Suppl.* **101** 537
[15] Motokawa M and Dohnomae H 1991 *J. Phys. Soc. Japan* **60** 1355
[16] Imamura N and Kobayashi T 1975 *J. Phys. Soc. Japan* **39** 829